J. Fluid Mech. (1996), *vol.* 326, *pp.* 125–150

Instabilities in quasi-two-dimensional magnetohydrodynamic flows

By L. BÜHLER

Forschungszentrum Karlsruhe, Institut für Angewandte Thermo- und Fluiddynamik
Postfach 3640, D-76021 Karlsruhe, Germany

(Received 8 August 1995 and in revised form 14 March 1996)

The improvement of heat transfer conditions in liquid-metal magnetohydrodynamic (MHD) flows is of prime importance for self-cooled fusion blanket design concepts. For many years the research was based on stationary inertialess assumptions since it was expected that time-dependent inertial flows would be suppressed by strong electromagnetic damping, especially in the extreme range of fusion relevant parameters. In the present analysis the stationary inertialess assumptions are abandoned. Nevertheless, the classical ideas usually used to obtain inertialess asymptotic solutions are drawn on. The basic inertial equations are reduced to a coupled two-dimensional problem by analytical integration along magnetic field lines. The magnetic field is responsible for a quasi-two-dimensional flow; the non-uniform distribution of the wall conductivity creates a wake-type profile, the MHD effect reducing to a particular forcing and friction. The solution for the two-dimensional variables, the field aligned component of vorticity, the stream function, and the electric potential are obtained by numerical methods. In a flat channel with non-uniform electrical wall conductivity, time-dependent solutions similar to the Kármán vortex street behind bluff bodies are possible. The onset of the vortex motion, i.e. the critical Reynolds number depends strongly on the strength of the magnetic field expressed by the Hartmann number. Stability analyses in viscous hydrodynamic wakes often use the approximation of a unidirectional flow which does not take into account the spatial evolution of the wake. The present problem exhibits a wake-type basic flow, which does not change along the flow path. It represents, therefore, an excellent example to which the simple linear analysis on the basis of Orr–Sommerfeld-type equations applies exactly. Once unstable, the flow first exhibits a regular time periodic vortex pattern which is rearranged further downstream. One can observe an elongation, pairing, or sometimes more complex merging of vortices. All these effects lead to larger flow structures with lower frequencies. The possibility for a creation and maintenance of time-dependent vortex-type flow pattern in MHD flows is demonstrated.

1. Introduction

In the past, liquid-metal magnetohydrodynamic (MHD) flows have been considered and investigated intensively as possible applications in self-cooled fusion reactors (e.g. Malang *et al.* 1988). The electrically conducting coolant suffers from an interaction of the flow with the strong, magnetic field confining the fusion plasma. Electric currents are induced in the fluid, which interact with the applied magnetic field. For strong magnetic fields the arising electromagnetic forces (Lorentz forces) are the dominant contribution to the momentum balance and the flow splits into distinct regions. The internal region is called the core, where the electromagnetic forces mainly balance the

pressure gradient. Inertial forces are very weak and viscous effects are confined to thin boundary layers at the walls. In recent years asymptotic methods have been considered as powerful computational tools for calculating the stationary, laminar, inertialess coolant flow in many three-dimensional geometries (see e.g. Bühler 1995; Molokov & Bühler 1994; Moon *et al.* 1992). For most applications in strong magnetic fields, inertia forces are small compared with Lorentz forces and have been taken into account in only a few works.

Heat transfer calculations based on laminar inertialess flows show that an intense enhancement of the convective heat removal from the plasma-facing wall would be desirable in order to keep the highest wall temperature below acceptable limits, to reduce the mean velocity, or to open the possibility for much simpler design options. An efficient improvement of heat transfer conditions by time-dependent turbulent motion may be inhibited by strong MHD damping where the kinetic energy of three-dimensional turbulent fluctuations is immediately removed by Joule's dissipation. On the other hand, MHD effects may intensify vortices whose axes are aligned with the magnetic field ('reversed energy cascade', see e.g. Sommeria & Moreau 1982; Sommeria 1986). Once created, such vortices are damped only weakly and can form quite large two-dimensional structures in the plane perpendicular to the magnetic field. The possibility of generating such vortices was mentioned several years ago (e.g. Kolesnikov & Tsinober 1972; Kolesnikov 1972). Andreev & Kolesnikov (1993) propose the use of so-called turbulence promoters (non-homogeneous wall conductivity) in order to initiate or intensify desired two-dimensional vortex patterns in the plane perpendicular to the magnetic field.

Although cited at other places in the present work it should be noted that the references listed above are not the first to deal with related phenomena in MHD flows. In 1956 Lehnert described an experiment in a rotationally symmetrical apparatus using a free-surface mercury layer above a highly conducting bottom. The bottom is split into several concentric rings, one of which is rotating. If the magnitude of an applied magnetic field is increased, the fluid in almost the whole device becomes stagnant, except that in a column located above the rotating part. Shear layers are formed and the motion, which was laminar without magnetic field becomes time-dependent, exhibiting vortex structures at the surface.

Abas (1969) analysed the stability of an MHD mixing layer. On the basis of an Orr–Sommerfield-type equation he finds that the onset of time-dependent motion in terms of the critical Reynolds number Re_c depends linearly on the strength of the applied magnetic field in terms of the Hartmann number M (for definition of these numbers see later in this paper).

Internal shear layer in MHD flows created by non-uniform electrical boundary conditions at the channel walls have attracted the attention of a number of researchers in the past. Alpher *et al.* (1960) describes an experiment using an open channel flow with a bottom wall of non-uniform conductivity. In the case of a highly conducting disk fixed at the bottom they observed an almost stagnant fluid column above the disk with its axis aligned with the applied strong magnetic field ('as though a fixed cylinder were immersed in the flow'). The interaction with the surrounding flow leads to a formation of a Kármán vortex street in the wake of the disk.

While in the experiment of Alpher *et al.* (1960) the electrodes act passively on the flow there are other active means to create or control MHD shear layers by applying voltage to electrodes placed at the walls. In a series of three subsequent papers Hunt & Williams (Part 1, 1968), Hunt & Malcolm (Part 2, 1968), and Hunt & Stewartson (Part 3, 1969) describe these types of flows. In the problem they consider, the electrodes

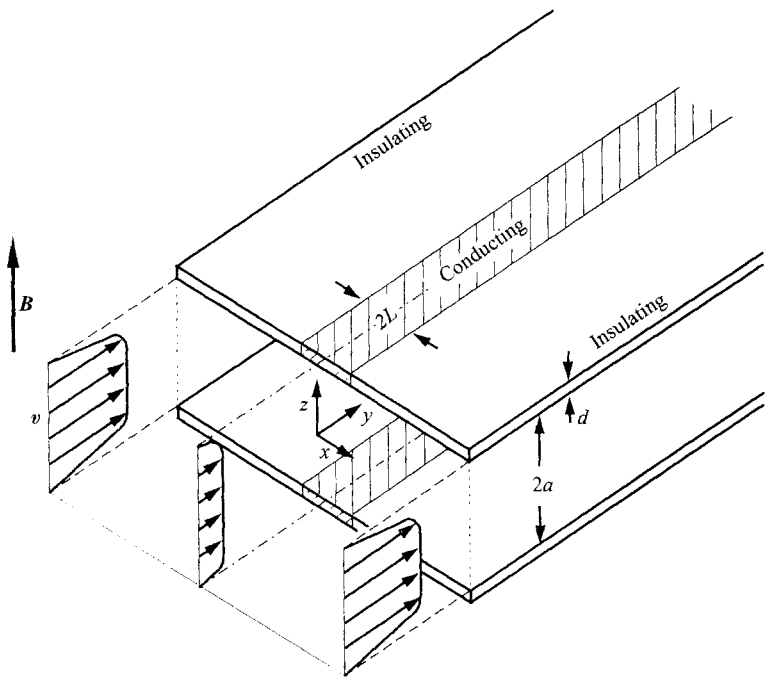

FIGURE 1. Geometry and coordinates.

create discontinuities in the electrical boundary conditions. Internal shear layers spread from these locations into the fluid along magnetic field lines, with characteristic thickness on the order of $M^{-1/2}$. In Part 1, the authors present an exact solution for the case of line electrodes and point electrodes at the walls and show a comparison with results of an asymptotic theory. In Part 2, results are shown for circular electrodes. A comparison of these results with a rotationally symmetric analysis (Part 3) confirms the theory, which predicts uniform flow variables along magnetic field lines with sharp shear layers starting at the electrodes edges. The instabilities of these shear layers are discussed by Malcolm (1970). He finds a stability limit (critical magnitude of current supplied to the electrodes) at which the basically steady state starts to exhibit time-dependent behaviour. In his paper Malcolm tries to relate the critical current to a critical Reynolds number. He finds for his experiment that $Re_c = const$ for moderate M and $Re_c \sim M^{1/3}$ as M is large.

In the present paper, we follow the idea of vortex generation by non-uniform conductivity of the channel walls with the aim of showing that an intense time-dependent mixing is possible or even favoured by the presence of a strong magnetic field. By the use of non-homogenous conductance at the walls of a flat channel (as suggested by Kolesnikov 1972 or earlier for the open channel flow by Alpher *et al.* 1960), a basic profile of velocity is created with two internal shear layers. The stability of this basically laminar unidirectional flow is considered. The nonlinear flow which establishes after the onset of a time-dependent motion is investigated by a numerical analysis.

The problem considered is the flow of an electrically conducting fluid under the influence of a strong, externally applied magnetic field. The flow is bounded by the parallel walls of a flat channel (see figure 1) similar to the problem treated by Hartmann

(1937) and by Chang & Lundgren (1961) for homogeneous conductance properties of the walls. As an extension of these fundamental works, the influence of an inhomogeneous conductivity of the walls is investigated. Abrupt changes of the wall conductivity lead to a formation of internal thin shear layers which spread from the point of discontinuity at the wall along magnetic field lines into the fluid. Such layers can carry a significant part of the total current which may lead to a complex three-dimensional current path causing interesting physical effects. Making theoretical predictions for such cases may be a difficult undertaking since all the nonlinear equations have to be solved by a detailed three-dimensional analysis resolving the internal layers.

To avoid these difficulties the inhomogeneities considered in the present paper have a smooth transition between the insulating condition as $|x| \gg L$ to highly conducting conditions within the strip of width $2L$. If the wall conductivity varies over distances large enough that internal layers do not occur (larger than the thickness of the internal layers), the possibility of analytically integrating the basic equations in the direction of the magnetic field is ensured. The integration of the basic equations in the magnetic field direction reduces the computational effort to the solution of a two-dimensional problem as in the case of the stationary inertialess core flow approximation. However, the time dependence associated with inertial effects in the plane perpendicular to the field are retained. This idea is not new and has been successfully applied (e.g. by Verron & Sommeria 1987) to study the MHD decay of initially given vortex patterns in insulating ducts. The present analysis is an extension of their ideas in order to investigate the time dependent inertial MHD flow in ducts with non-uniform wall conductivity. The main interest is focused on the question of whether there are possibilities for vortex generation and what will be their nonlinear interaction once they are created.

2. Formulation

The considered flow of an electrically conducting fluid is assumed to be inductionless and governed by the following set of equations (e.g. Sommeria & Moreau 1982) for conservation of

mass
$$\nabla \cdot \boldsymbol{v} = 0, \tag{2.1}$$

momentum
$$\partial_t \boldsymbol{v} + (\boldsymbol{v} \cdot \nabla)\boldsymbol{v} = -\nabla p + \frac{1}{Re}\Delta \boldsymbol{v} + N\boldsymbol{j} \times \hat{\boldsymbol{z}}, \tag{2.2}$$

charge
$$\nabla \cdot \boldsymbol{j} = 0, \tag{2.3}$$

and by Ohm's law
$$\boldsymbol{j} = -\nabla \phi + \boldsymbol{v} \times \hat{\boldsymbol{z}}. \tag{2.4}$$

Here $\boldsymbol{v} = (u, v, w)$, $\boldsymbol{j} = (j_x, j_y, j_z)$, ϕ, p denote velocity, current density, electric potential and pressure, scaled with a characteristic velocity V, with σVB, VLB, and ρV^2, respectively. σ and ρ are the electric conductivity and density of the fluid, B the magnitude of the constant, uniform magnetic field $B\hat{\boldsymbol{z}}$, and L is a characteristic scale in the transverse (the x-) direction.

The problem is characterized by two independent parameters. The Reynolds number $Re = VL/\nu$ represents the ratio of inertia and viscous effects where ν is the kinematic viscosity. The interaction parameter $N = \sigma LB^2/\rho V$ also known as the Stuart number gives the ratio of electromagnetic and inertia forces.

The fluid is bounded by two parallel walls at $z = \pm a$ which are perpendicular to the

magnetic field. The boundary conditions at the upper fluid–wall interface are the no-slip condition

$$\boldsymbol{v} = 0 \quad \text{at} \quad z = a, \tag{2.5}$$

and the thin-wall condition (see e.g. Walker 1981)

$$\boldsymbol{j}\cdot\hat{\boldsymbol{z}} = -\nabla_{xy}\cdot\left(\frac{\sigma_w}{\sigma}\mathrm{d}\nabla_{xy}\phi\right) \quad \text{at} \quad z = a. \tag{2.6}$$

Currents leaving the fluid region at $z = a$ enter the wall of non-dimensional thickness d. They turn in tangential direction and create in the wall a distribution of potential according to (2.6). The ratio of wall to fluid conductivity is σ_w/σ. ∇_{xy} stands for the projection of the gradient vector in the (x, y)-plane.

The same inhomogeneity of the wall conductivity is assumed to be present at the top and bottom wall so that the entire problem is symmetric with respect to the plane $z = 0$. Therefore, only the upper half of the channel is considered with appropriate symmetry conditions

$$\partial_z u = \partial_z v = w = 0 \quad \text{at} \quad z = 0, \tag{2.7}$$

$$\boldsymbol{j}\cdot\hat{\boldsymbol{z}} = 0 \quad \text{at} \quad z = 0. \tag{2.8}$$

At the lateral boundaries the flow is unidirectional and fully developed with

$$\boldsymbol{v} = v(z)\cdot\hat{\boldsymbol{y}} \quad \text{as} \quad x \to \pm\infty, \tag{2.9}$$

according to Hartmann's solution.

For stability investigations the flow is assumed to satisfy periodic boundary conditions at the inlet and outlet. For studying global nonlinear phenomena the flow is assumed to be fully developed at the inlet to the computational domain. At the end as $y \to \infty$, a kind of free outflow condition is used. This condition will be discussed later.

3. Reduction to a two-dimensional problem

The elimination of pressure from (2.2) leads to the equation

$$\nabla\times[\partial_t\boldsymbol{v} + (\boldsymbol{v}\cdot\nabla)\boldsymbol{v}] = \frac{1}{Re}\nabla\times\Delta\boldsymbol{v} + N\partial_z\boldsymbol{j}, \tag{3.1}$$

which clearly demonstrates the strong correlation of the variables along magnetic field lines for large values of N and Re.

$$\partial_z\boldsymbol{j}_c \to 0 \quad \text{for} \quad Re > 1, \quad N \to \infty. \tag{3.2a}$$

Moreover, by taking the curl of (3.1) twice and using Ohm's law it can be shown that

$$\partial_{zz}\boldsymbol{v}_c \to 0 \quad \text{for} \quad Re > 1, \quad N \to \infty. \tag{3.2b}$$

Using the symmetry conditions at $z = 0$ the relations

$$\partial_z\phi_c = \partial_z u_c = \partial_z v_c = w_c = 0, \tag{3.2c}$$

which are valid in the whole core, can be deduced immediately for large N as a direct consequence of conditions (3.2a, b). The superscript c denotes variables in the core. This means that the vorticity $\boldsymbol{\Omega} = \nabla\times\boldsymbol{v}$ has only one component $\boldsymbol{\Omega}_c = \Omega_{cz}\hat{\boldsymbol{z}}$ in the core, aligned with the magnetic field. Please note that the symmetry condition at the plane $z = 0$ is convenient but not necessary. In the more general case one simply has to determine the influence of viscous friction and Joule's dissipation in both viscous boundary layers at the walls separately and to study their common impact to the flow in the core.

In the viscous boundary layers at the walls, called the Hartmann layers, additional contributions to the vorticity are necessary to satisfy the no-slip condition. With the abbreviation $\Omega_{\delta z}$ for the viscous correction to the field-aligned component of vorticity (in addition to the core solution Ω_{cz}), after a stretching of the wall normal coordinate, one gets the boundary-layer equation

$$\frac{1}{Re}\frac{1}{\delta^2}\partial_{\zeta\zeta}\Omega_{\delta z} - N\Omega_{\delta z} = 0. \tag{3.3}$$

Equation (3.3) has been derived assuming that the core variables satisfy the inviscid part of (3.1). Further it has been assumed that the potential ϕ does not vary across the boundary layer, i.e. the viscous correction for potential vanishes to the main order of approximation (see e.g. Moreau 1990, p. 128). The first term of (3.3) is obtained from the viscous term of (3.1) by introducing a stretched boundary-layer coordinate. The second term results if $\partial_z j_z$ is expressed via the charge conservation equation (2.3) by the current components j_x, j_y using Ohm's law (2.4). The scale of the stretched wall normal coordinate $\zeta = z/\delta$ turns out to be on the order $\delta = (Re\,N)^{-1/2}$ for a reasonable balance of forces. The quantity $(Re\,N)^{1/2} = Ha$ corresponds to the well-known Hartmann number. Equation (3.3) happens to be independent of the x and y coordinates. Its solution matches the core values Ω_{cz} exponentially with the no-slip condition.

The behaviour of velocity components determined by (3.2c) and (3.3) justify the representation of the fluid velocity by

$$u = -\partial_y \psi(x,y) f(z), \quad v = \partial_x \psi(x,y) f(z), \quad w = 0, \tag{3.4a–c}$$

using the two-dimensional stream function $\psi(x,y)$. The separated form (3.4) with a function f independent of the x- and y-coordinates is indeed a strong assumption and not valid in general. Nevertheless, it should be valid for very strong magnetic fields as $N \gg 1$ or in the Hele-Shaw approximation as $a \ll 1$. The above arguments may be good or best for laminar flows. However, even time-dependent flows should approximately be described by (3.4) as long as the velocity in the magnetic field direction is negligibly small and a strong correlation along field lines of the velocity components perpendicular to the field is observed. Since this has been the case in several MHD experiments reported in the past by a number of authors, there is evidence that assumption (3.4) is valid for strong fields unless the flow becomes really three dimensional (see also the discussion in § 5.3).

Equations (3.4a–c) determine the velocity field in the core and in the Hartmann layers for $Re \gg 1$ and $N \gg 1$. The shape function $f(z)$ has to satisfy the no-slip condition $f(a) = 0$ and the symmetry condition $\partial_z f(0) = 0$. Owing to the normalization $\int_0^a f\mathrm{d}z = a$ the velocity scale V introduced earlier is the z-averaged velocity as $x \to \pm\infty$. For this case, f corresponds to the solution of Hartmann's problem $\boldsymbol{v} = f(z)\hat{\boldsymbol{y}}$ as $x \to \pm\infty$.

With the definitions (3.4), equation (3.1) for the z-component of vorticity $\Omega_z = \omega(x,y)f = \Delta_{xy}\psi f$ reads

$$\partial_t \omega f + f^2(\partial_x \psi \partial_y \omega - \partial_y \psi \partial_x \omega) = \frac{1}{Re}\Delta_{xy}\omega f + N\left[\left(\frac{\partial_{zz} f}{Ha^2} - f\right)\omega + \Delta_{xy}\phi\right], \tag{3.5}$$

The Ohm's law and the charge conservation equation have been combined to give

$$\partial_z j_z = \Delta_{xy}\phi - \omega f, \tag{3.6}$$

an expression which has been already used to derive (3.5).

For high values of N, (3.5) has the asymptotic limit

$$\partial_{zz} f - Ha^2 f = \text{function}\,(x,y) \quad \text{as} \quad N \to \infty, \tag{3.7a}$$

from which the function f is determined as

$$f = 1 - e^{Ha(z-a)} \quad \text{for} \quad Ha \gg 1, \tag{3.7b}$$

while for very small values of Ha the asymptotic solution corresponds to the Hele-Shaw approximation

$$f(z) = \frac{3}{2}\left[1 - \left(\frac{z}{a}\right)^2\right] \quad \text{if} \quad a \ll 1. \tag{3.7c}$$

The Hele-Shaw approximation usually applies for flows confined between two parallel plates with a distance much smaller than the transverse characteristic dimension, if $a \ll 1$. In the present paper, the applications of the theory, however, focus on high Hartmann numbers so that the hydrodynamic limit is not considered further.

Both equations (3.5) and (3.6) are integrated in the z-direction. The analytical integration along field lines has been used by many authors, e.g. Lavrent'ev *et al.* (1990) to determine inertialess MHD flows. The integration is performed taking into account the thin-wall condition (2.6) and $\partial_z f = -Ha$ at $z = a$ for strong magnetic fields ($Ha \gg 1$) and the symmetry conditions at $z = 0$. Neglecting higher-order terms $O(1/Ha)$ one ends up with the two-dimensional equations

$$\Delta_{xy}\psi = \omega, \tag{3.8}$$

$$\nabla_{xy}\cdot([1+c]\nabla_{xy}\phi) = \omega, \tag{3.9}$$

$$\partial_t\omega + \partial_x\psi\,\partial_y\omega - \partial_y\psi\,\partial_x\omega = \frac{1}{Re}\Delta_{xy}\omega - \frac{\omega}{\tau} - \frac{N}{1+c}\nabla_{xy}c\cdot\nabla_{xy}\phi, \tag{3.10}$$

determining the stream function, the electric potential and the vorticity, with the lateral boundary conditions

$$\partial_x\psi = (1+c)\,\partial_x\phi = 1, \quad \omega = 0 \quad \text{as} \quad x \to \pm\infty. \tag{3.11}$$

The wall conductance ratio $c = \sigma_w d/\sigma a$ characterizes the integral importance of the wall to fluid conductivity. The resulting flow in the core is two-dimensional with the MHD effects of the three-dimensional problem expressed in a special friction and forcing term.

The left-hand side of (3.10) describes the time-dependent convective transport of vorticity. The right-hand side contains two dissipation terms, one describing viscous losses due to transverse gradients of vorticity and the other one accounting for Joule's dissipation in the Hartmann layer and in the thin wall. The latter one may become dominant at high Reynolds number. τ is a characteristic timescale for the decay of vorticity due to Joule's dissipation. Using the rescaled Hartmann number $M = aHa$, it is defined as

$$\tau = \left(\frac{N}{M} + \frac{cN}{1+c}\right)^{-1} \tag{3.12}$$

and exhibits the asymptotic limits

$$\tau \to \begin{cases} M/N = a(Re/N)^{1/2} & c \ll M^{-1}, \\ (cN)^{-1} & \text{for} \quad M^{-1} \ll c \ll 1, \\ N^{-1} & c \gg 1, \end{cases} \tag{3.13}$$

which clearly demonstrate that vortices in highly conducting channels ($c \gg 1$) are damped very rapidly. For moderate values of the wall conductance ratio, the life time of a vortex can become much larger, so that it may exist over a certain period even if

the interaction parameter is large. The weakest damping occurs in almost insulating ducts when $c \ll M^{-1}$. For such conditions the decay time becomes very large if the Reynolds number or the aspect ratio a are large. For insulating duct walls with $c = 0$ the decay time τ is determined only by the breaking due to the Hartmann layers (see e.g. Moreau 1990). The general concept of the two-dimensional disturbances' decay being determined by the Hartmann layer on a scale proportional to Re/M was pointed out already by Shercliff (1965) and others.

For $c = const$, (3.10) becomes independent of the potential equation and can be solved without knowing the potential distribution. For this case the vorticity equation is comparable to the equation used by Verron & Sommeria (1987) for the case $c = 0$.

The last term of (3.10) is a source term of vorticity and describes the vorticity generation at positions where the wall conductance ratio varies. This is exactly the case near both sides of the conducting strip. In contrast to previous works which considered only the MHD vortex decay, (3.10) accounts for vorticity production in addition.

Both last terms in (3.10) have been brought into the equation by the boundary conditions of the original three-dimensional problem and give rise to shear layers aligned with the magnetic field. It should be mentioned that in the paper by Verron & Sommeria (1987), there is a source term, proportional to the current density j_z at the wall. By using the thin wall condition and Ohm's law we can express the transverse current in their analysis and completely recover (3.8)–(3.10).

4. Linear stability analysis

If the wall conductance ratio is a function of the transverse coordinate only, $c = c(x)$ equations (3.8)–(3.11) are satisfied by a basic unidirectional flow $\psi_0(x)$, $\phi_0(x)$, $\omega_0(x)$. The general time-dependent solution is expanded in normal modes as $\psi(x, y, t) = \psi_0(x) + \psi_1(x) e^{ik(y-st)}$ for stream function and in an analogous way for potential and vorticity. The wavenumber k and the phase velocity s in general have complex values. If one is interested in the temporal growth of spatially periodic flows, k is usually assumed to be real, while $s = s_r + is_i$ is complex. The imaginary part s_i determines whether a solution is amplified or damped in time, if $s_i > 0$ or $s_i < 0$, respectively. The real part s_r of the phase velocity gives the travelling speed in the y-direction of a flow pattern. Time periodic solutions are characterized by a real valued frequency sk and by a complex wavenumber $k = k_r + ik_i$ of which the imaginary part determines the spatial growth rate. Temporal and spatial analyses lead to the same stability limits of the basic flow since their results coincide at the neutral limit of stability $s_i = k_i = 0$. The results for the neutral modes obtained by the temporal analysis outlined in this section apply, therefore, as well for the neutral spatial modes. If one is interested whether an unstable solution is convectively unstable, or absolutely unstable in the sense of the terminology used in several works (see e.g. Huerre & Monkewitz 1985; Monkewitz 1988; Hannemann & Oertel 1989) a pure temporal analysis would not be sufficient. The flow is called convectively unstable if an amplified perturbation moves downstream with the flow, while it is absolutely unstable if disturbances grow in time at the place where they were initiated.

With the abbreviation $D = \partial_x$ the equations (3.8)–(3.10) read:

$$(D^2 - k^2)\psi_1 = \omega_1, \tag{4.1}$$

$$(DcD + [1 + c](D^2 - k^2))\phi_1 = \omega_1, \tag{4.2}$$

$$(D\psi_0 - s)\omega_1 - D\omega_0\psi_1 = -\frac{i}{k}\left[\left(\frac{D^2 - k^2}{Re} - \frac{1}{\tau}\right)\omega_1 - \frac{N}{1+c} DcD\phi_1\right], \tag{4.3}$$

with boundary conditions $\psi_1 = \phi_1 = \omega_1 = 0$ as $x \to \pm\infty$, assuming that the corrections to the basic flow are small. For pure hydrodynamic flow, $N \to 0$, (4.3) would find its limit in the classical Orr–Sommerfeld equation. Equations (4.1)–(4.3) constitute an eigenvalue problem for the complex phase velocity s. The same equations with $k = 0$ first serve for the determination of the basic flow if $\psi_1 = \phi_1 = \omega_1$ are replaced by $\psi_0 = \phi_0 = \omega_0$ and boundary conditions (3.11) are applied.

The set of equations (4.1)–(4.3) is solved numerically by an iterative method for fixed values of the physical parameters Re, N and given wavenumber k and wall conductance ratio $c(x)$. First, a mapping $x(u) = x_{\max} \sinh \beta u / \sinh \beta$ in the x-direction is introduced. The geometric parameter β ensures a high resolution in the region near the conducting strip while near the sides, where the values and derivatives of $\psi_1 = \phi_1 = \omega_1$ vanish, a lower resolution will have less influence on the accuracy. The computational domain ends laterally at $x = \pm x_{max}$, a value which is chosen large enough that the boundary conditions, which are valid as $x \to \pm\infty$, hold with sufficient accuracy. After the mapping, all derivatives are expressed by finite differences.

Starting from an initial guess (subscript n) an improved solution (subscript $n+1$) is calculated by

$$\omega' = (s^{n+1} - s_0)\,\omega_1^n = F(k, \psi_0, \omega_0; \psi_1^n, \phi_1^n, \omega_1^n) - s_0\,\omega_1^n, \tag{4.4}$$

from which $s^{n+1} - s_0$ is evaluated as

$$s^{n+1} - s_0 = \frac{\int \omega' \cdot \omega' \,\mathrm{d}x}{\int \omega_1^n\, \omega' \,\mathrm{d}x}. \tag{4.5}$$

The integration is performed between the lateral boundaries of the computational domain. Once s^{n+1} is known ω' is normalized to give ω_1^{n+1}. The function F corresponds to (4.3) transformed to $s\omega_1 = F$. The value s_0 has been introduced in order to avoid numerical instabilities during the iteration process. Equations (4.1) and (4.2) are used to determine ψ_1^{n+1} and ϕ_1^{n+1}. The iteration is performed until the changes in the eigenvalue are sufficiently small, e.g. 10^{-8}.

Equation (4.3) may be satisfied by a number of eigenvalues s with corresponding eigenfunctions ψ_1, ϕ_1, ω_1. For stability considerations the eigenvalue s with highest value of s_i is required. This can be achieved with a proper choice of s_0. The fact that the obtained eigenvalue is the relevant one for the onset of instability is confirmed later by a two-dimensional nonlinear numerical analysis.

For the following discussion of results a reference case is defined with $M = 10^3$, $a = 10$. The wall conductance ratio varies according to $c(x) = c_0/[1 + (\sinh x/\sinh x_0)^m]$, with $c_0 = 10^{-2}$, $x_0 = 1$, $m = 6$. The variation is shown in figure 2(*a*). As a result of the higher wall conductance ratio near $x = 0$ the velocity $v_0 = \partial_x \psi_0$ of the basic flow is reduced (see figure 2*b*). The reduction of velocity can be approximately described by the formula according to Chang & Lundgren (1961), neglecting higher-order terms $O(1/M)$.

$$v_0 = \frac{c+1}{Mc+1}. \tag{4.6}$$

As a consequence two layers occur at the right- and at the left-hand side of the conducting strip with two peaks of vorticity. This basic flow is independent of the Reynolds number Re if M, c and a remain unchanged. The Reynolds number therefore, represents a physical parameter which can be used to investigate the stability of the same basic flow. Alternatively, instead of Re the parameter N could be used.

The limits of stability are characterized by the neutral curves defined as $s_i(k, Re, M, \ldots) = 0$, which for a given set of physical parameters separate the region of

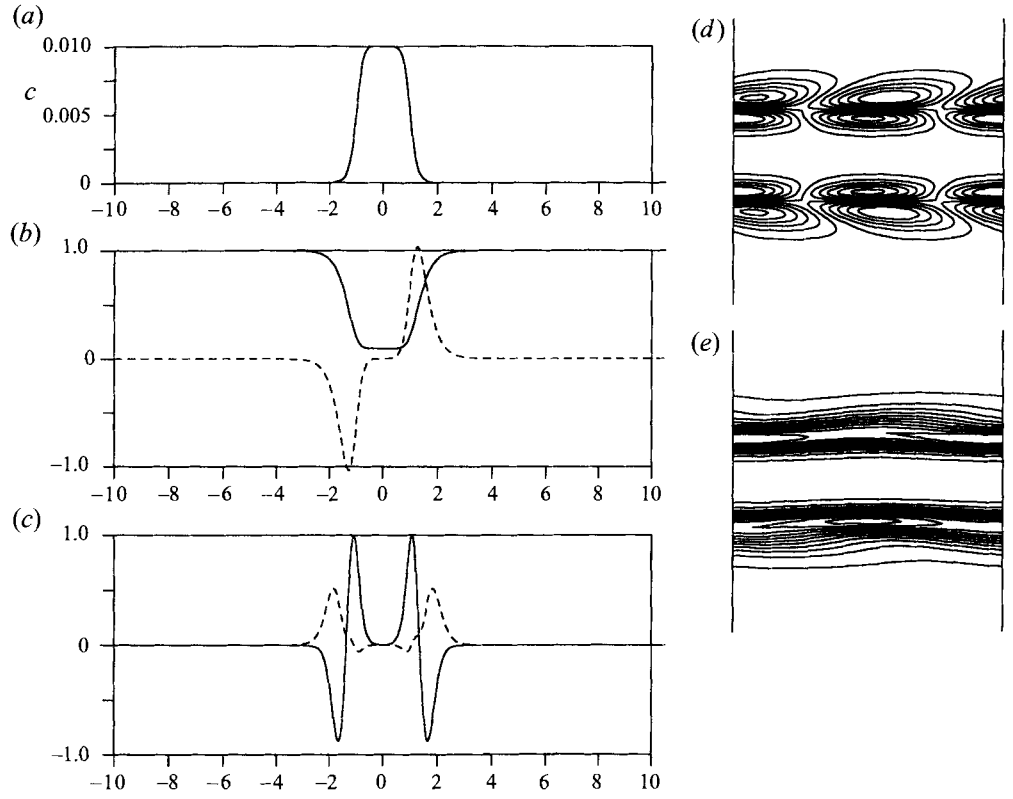

FIGURE 2. Fully developed flow and eigensolution at the limit of stability. $M = 10^3$, $Re_c = 182$, $k_c = 0.783$, $\lambda_c = 8.02$. (*a*) Distribution of wall conductance ratio, (*b*) basic solution for ——, the unidirectional velocity v_0 and – – –, vorticity ω_0, (*c*) ——, real and – – –, imaginary part of the eigensolution ω_1, (*d*) isolines of $\omega_1 \exp(ik_c y)$, (*e*) isolines of superposition of $\omega_0 + 0.2\,\omega_1 \exp(ik_c y)$.

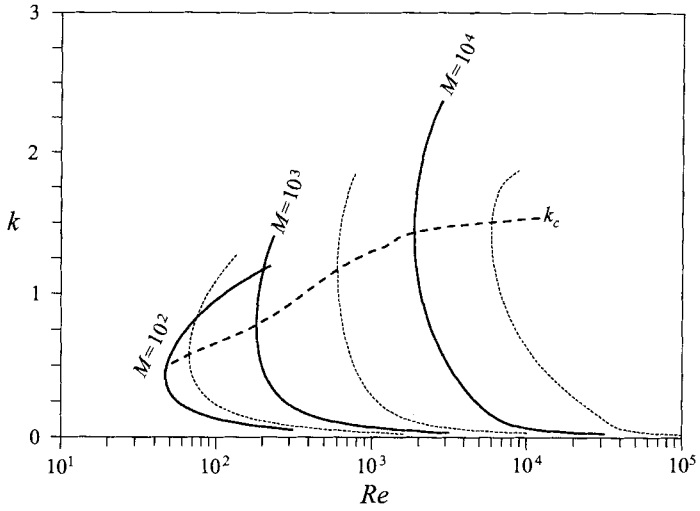

FIGURE 3. Curves of neutral stability. Stable regions are at the left-hand side, unstable regions are at the right-hand side of the curves.

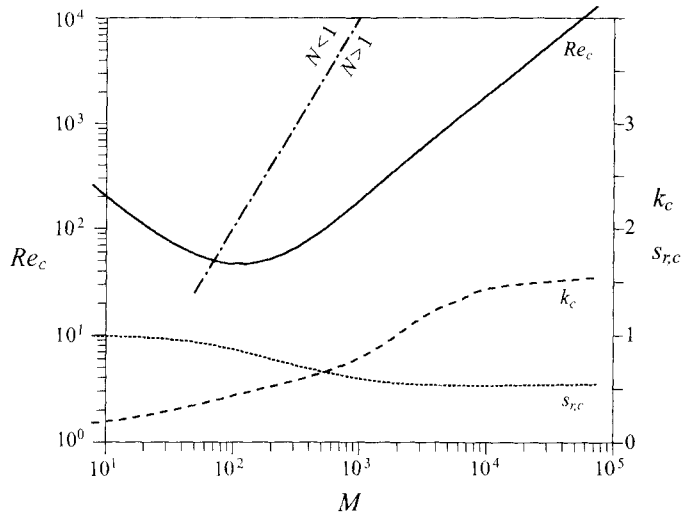

FIGURE 4. Critical values ——, Re_c; – – –, k_c; · · · ·, $s_{r,c}$; – · – · –, $Re(N = 1)$; only values of Re below this line satisfy the model assumption.

wavenumbers for which small perturbations are damped from those creating amplified solutions. Results are summarized in figure 3. In addition to the reference case $M = 10^3$, neutral stability curves for other values $M = 10^\alpha$, $2 \leqslant \alpha \leqslant 4.5$ are shown.

The flow is stable for a given set of parameters if the combination of (k, Re) is at the left-hand side of the neutral curves while it is unstable if (k, Re) lies at the right-hand side of the curves. For a given M the flow is stable against perturbations with any wavenumber $0 < k < \infty$ if Re is smaller than a critical value Re_c given by the vertical tangent to the neutral curve. If the Reynolds number is slightly higher, the instability will be initiated with the critical wavenumber k_c. The dashed curve indicated in figure 3 represents the critical values for (Re_c, k_c) which are a function of the parameter M.

The values of Re_c as a function of M are plotted in figure 4 together with the wave number k_c and the real part of the phase velocity $s_{r,c}$. It turns out that Re_c becomes proportional to M for large values of M. This fact is to be expected if (4.3) is considered. For high Re, the eigenvalue problem becomes directly independent of Re. The most important parameter governing the stability problem becomes τ. The limit of stability depends therefore only on a characteristic value τ_c. A fixed value of τ_c, which is approximately proportional to Re/M since almost the whole computational domain is insulating, will lead to the result above. It is remarkable that the ratio Re/M has been found to be a characteristic property for the onset of turbulent motion in several MHD experiments since the early 1960s. A short summary of these results is given by Moreau (1980), more details can be found in the review presented by Lielausis (1975). The fact that the loss of laminar stability in these experiments happens to occur for $Re > Re_c \sim M$, as in the present theory, supports the idea that the first transition leads to quasi-two-dimension time-dependent motion once a critical value for a two-dimensional stability criteria is exceeded. Indeed, Kolesnikov & Tsinober (1974, cited e.g. by Moreau 1990, p. 289) could clearly prove that the turbulent motion exhibits strong two-dimensional features.

For smaller values of M the critical value Re_c deviates from this dependency and reaches a minimum near $M = 10^2$. The reason for the stabilizing effect for $M < 10^2$ is the following: The driving mechanism for instabilities is the velocity deficit across the

shear layers. From (4.6) it is obvious, that for $M < c^{-1}$ this deficit and thus the destabilization becomes continuously weaker. The figure contains also the line $Re(N = 1, M)$ which should remind the reader about the limits of application of the present model since it has been assumed that $N \gg 1$ (say one order of magnitude). If this condition is not satisfied the analysis should be really three-dimensional, but it is expected that the present quasi-two-dimensional results still hold qualitatively. The value of k_c increases and that of $s_{r,c}$ decreases continuously with increasing M in the range of parameters considered. For small values of M, the characteristic transport velocity is $s_{r,c} = 1$, while for large $M, s_{r,c}$ approaches a value slightly higher than 0.5. Both values correspond approximately to the velocity at the position with highest magnitude of vorticity, a position at which the instability is initiated.

The eigensolution for ω_1 for the reference case at the limit of stability $Re_c = 182$, $k_c = 0.783$ is shown in figure 2(*c*) as a function of x. A better insight into the physics is provided by figure 2(*d*) where isolines of $\omega_1 \exp(ik_c y)$ are plotted in the (x, y)-plane for one wavelength $\lambda_c = 2\pi/k_c$. In a superposition of the eigensolution with the basic flow, shown in figure 2(*d*), the wavy type of the full solution can be seen.

The following chapter is concerned with the nonlinear solution of the model equations (3.8)–(3.10) with boundary conditions (3.11). Results are compared with those obtained by the linear theory in order to validate both independent methods.

5. Nonlinear numerical analysis

Further investigations are focused on the nonlinear, time-dependent development of the flow. Since the numerical procedure is more or less standard, only some basic ideas are presented before the discussion of results. For convenience the same mapping in the transverse direction has been used as for the stability analysis to ensure a high numerical resolution near the shear layers. The vorticity equation (3.10) is used in the form

$$\partial_t \omega + \frac{\omega}{\tau} = J(\omega, \psi) + \frac{1}{Re}\Delta_{xy}\omega - \frac{N}{1+c}\nabla_{xy} c \cdot \nabla_{xy}\phi. \tag{5.1}$$

where $J(\omega, \psi) = \partial_y \psi \partial_x \omega - \partial_x \psi \partial_y \omega$. The Jacobian $J(\omega, \psi)$ is approximated by the scheme proposed by Arakawa (1966). This scheme which conserves the mean square of kinetic energy and the mean square vorticity is a robust tool for the approximation of the nonlinear terms even at high Reynolds numbers.

The right-hand side of (5.1), for simplicity abbreviated to $R(t)$, is approximated by finite differences and linearized in time in the form of a linear extrapolation from two previous timesteps t_n and $t_{n-1} = t_n - \Delta t$. The equation (5.1) is integrated analytically in time between t_n and $t_{n+1} = t_n + \Delta t$ with the linearized right-hand side $R(t) = R(t_n) + [R(t_n) - R(t_{n-1})]t/\Delta t$ to give $\omega(t_{n+1})$. The time integration proposed converges to the Adams–Bashforth scheme as $\Delta t/\tau \to 0$. Once $\omega(t_{n+1})$ is known $\psi(t_{n+1})$ and $\phi(t_{n+1})$ are calculated according to (3.8) and (3.9) using a fast Poisson solver.

Tests of convergence of the numerical scheme for the reference case with $M = 10^3$, $a = 10$, and $Re = 500$ showed that between the grids $(n_x \times n_y) = (40 \times 10)$, (60×20), (80×30), and (100×40) the relative changes of a typical signal $\langle E_x \rangle$ (see equation (5.3) below) decreases from 3.3%, 0.72% to 0.019%. This indicates that even $n_x = 60$ grid points in the x-direction and $n_y = 20$ grid points in the y-direction over one wavelength are enough to describe the flow with sufficient accuracy. Nevertheless, most calculations have been performed with $n_x \geqslant 100$ and more than 20 points per wavelength in the y-direction.

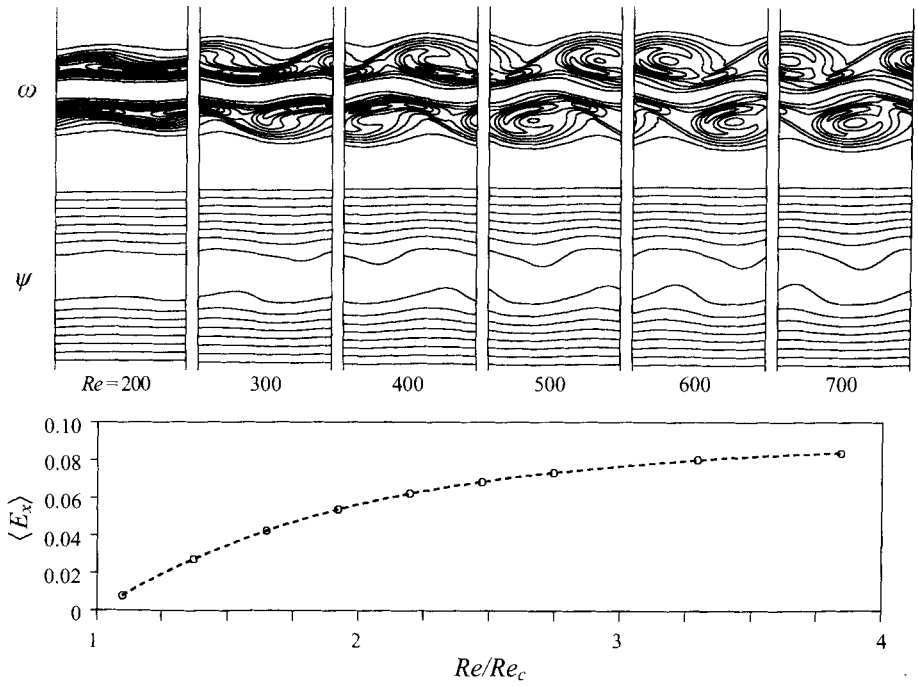

FIGURE 5. Nonlinear periodic solution with wavelength $\lambda_c = 8.02$ for several values of Re. The data points in the diagram for the averaged kinetic energy $\langle E_x \rangle$ correspond to the solutions for vorticity ω and streamfunction ψ as shown above. Re_c has been evaluated by the linear theory to $Re_c = 182.07$.

5.1. *Periodic solutions in space*

The first nonlinear numerical calculations have been performed with periodic boundary conditions between the inlet and outlet of the computational domain in order to have a possibility for a direct comparison between nonlinear results and the results obtained by the linear theory. To characterize the local magnitude or intensity of an unstable time-dependent flow, the kinetic energy in the transverse direction E_x at a cross-section y is used.

$$E_x(y,t) = \int_{-x_{max}}^{x_{max}} \frac{1}{a} \int_0^a u^2 \,\mathrm{d}z \,\mathrm{d}x = \int_{-x_{max}}^{x_{max}} (\partial_y \psi)^2 \,\mathrm{d}x. \tag{5.2}$$

For flows with periodic boundary conditions at the inlet and outlet an averaged value

$$\langle E_x(t) \rangle = \frac{1}{\lambda} \int_y^{y+\lambda} E_x(y,t) \,\mathrm{d}y \tag{5.3}$$

gives a space independent measure for the intensity of a vortex pattern which travels through the computational domain. After the flow has reached its nonlinear saturation $\langle E_x \rangle$ becomes independent of time.

The first nonlinear calculations are performed to get data for a comparison with the linear stability analysis in order to confirm the physical relevance of the obtained eigenvalues and to validate the nonlinear numerical scheme. Calculations are started with the reference case as used for presentation of results of the linear stability analysis ($M = 10^3$ and $a = 10$). The length of the computational domain for the nonlinear analysis has been fixed to the critical wavelength $\lambda_c = 2\pi/k_c = 8.02$ obtained from the linear stability analysis. Results are shown in figure 5 for stream function ψ and for

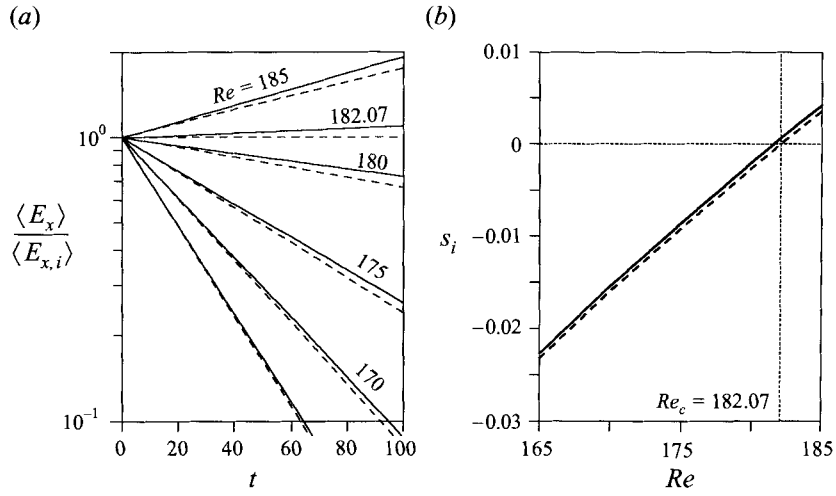

FIGURE 6. Comparisons of results obtained by ——, the numerical nonlinear code by – – –, the linear stability analysis for the reference case $M = 10^3$, $a = 10$ with $k = k_c = 0.783$. (*a*) Time history of damped or amplified nonlinear solutions for the same initial condition for several values of *Re*. (*b*) s_i as a function of *Re*.

vorticity ω in form of instantaneous isolines for fully established conditions at Reynolds number $200 \leqslant Re \leqslant 700$. The flow at $Re = 200$ is already unstable and shows a wavy solution for ψ and ω which travels through the computational domain in the main flow direction. As *Re* increases nonlinear effects become more important and a formation of regions with local maxima of vorticity becomes visible. With decreasing *Re* the averaged transverse kinetic energy decreases continuously, indicating that at $Re = Re_c$, based on the linear stability analysis, any transverse motion will stop.

To fix the critical Reynolds number with higher accuracy by the nonlinear numerical method, the time history of $\langle E_x(t) \rangle$ of transient solutions is considered. The nonlinear analysis is started with initial conditions (subscript *i*)

$$(\omega, \psi, \phi)_i = (\omega, \psi, \phi)_0 + \epsilon(\omega, \psi, \phi)_1 \, e^{ik(y-st)}.$$

Here, ϵ is a small, initial perturbation amplitude. The transverse kinetic energy is amplified or damped according to the linear analysis as

$$\langle E_x(t) \rangle = \langle E_{x,i} \rangle \exp(2ks_i t), \tag{5.4}$$

where $\langle E_{x,i} \rangle$ is the mean transverse kinetic energy of the initial condition. The left-hand side is evaluated using the two-dimensional numerical calculations and compared with the right-hand side obtained by the linear theory. Figure 6(*a*) shows results for $\langle E_x \rangle$ which have been obtained by the linear theory (dashed lines) and by the nonlinear numerical code (solid lines) for several values of *Re* near the critical value Re_c. Solutions for $Re < Re_c$ are damped, those for $Re > Re_c$ are amplified.

The slopes in the diagram with the linear-logarithmic axis determines the imaginary part s_i of the phase velocity

$$s_i = \frac{\ln(\langle E_x(t) \rangle / \langle E_{x,i} \rangle)}{2k_c t}. \tag{5.5}$$

The values of s_i obtained with the nonlinear numerical method are compared with

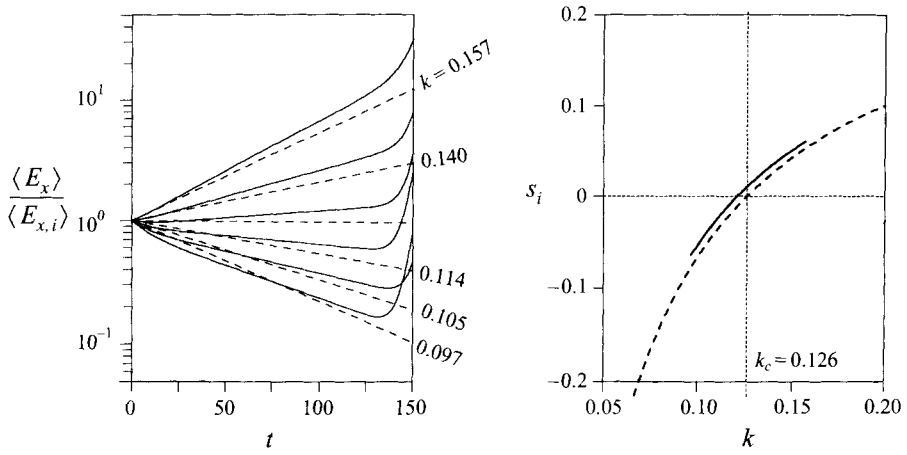

FIGURE 7. Comparison of results obtained by ——, the numerical nonlinear code and by – – –, the linear stability analysis for the reference case $M = 10^3$, $a = 10$ with $Re = 500$. (*a*) Time history of damped or amplified nonlinear solutions for the same initial condition for several values of k. (*b*) s_i as a function of k.

those obtained by the linear theory in figure 6(*b*). The values of the critical Reynolds number, for which $s_i(Re_c) = 0$, are found to be in very good agreement for both methods.

Similar agreement is found for the reference case $M = 10^3$, $a = 10$, if the Reynolds number is fixed to the value $Re = 500$ in order to analyse the range of stable or unstable wavenumbers. Figure 7 shows the time history of damped or amplified signals obtained by the linear theory and by the nonlinear numerical code. The slopes in figure 7(*a*) which determine the amplification rate of a perturbed solution are summarized in figure 7(*b*). The agreement of results obtained by the nonlinear theory and by the linear stability analysis is good. For larger times ($t > 125$), faster growing eigenmodes become more important than the investigated basic mode. The reason is that these modes which also lie in the unstable region of the stability diagram (figure 3) are not excluded by the nonlinear analysis and, once initiated, grow faster than the investigated basic mode with smaller wavenumber.

5.2. *Defined inflow, free outflow*

More relevant for experimental or engineering applications are conditions of defined inflow and free outflow. As inflow conditions at $y = 0$, the solution ψ_0, ϕ_0, ω_0 of equations (3.8)–(3.10) is given, assuming a fully established flow, i.e. $\partial_y = 0$. At the outflow boundary the conditions

$$\partial_t \begin{pmatrix} \psi \\ \phi \end{pmatrix} + v\,\partial_y \begin{pmatrix} \psi \\ \phi \end{pmatrix} = \begin{pmatrix} 0 \\ 0 \end{pmatrix} \quad \text{at} \quad y = y_{max} \tag{5.6}$$

are introduced for stream function ψ and for potential ϕ. These conditions describe the undisturbed convective transport of the exit flow pattern in the main flow (the y-) direction. Equation (3.10) for the vorticity ω can be directly evaluated at the outflow boundary, neglecting viscous terms on the order Re^{-1} in the axial direction. This assumption may cause a boundary layer at the exit. However, its influence on the flow within the computational domain should be negligibly small for high values of Re.

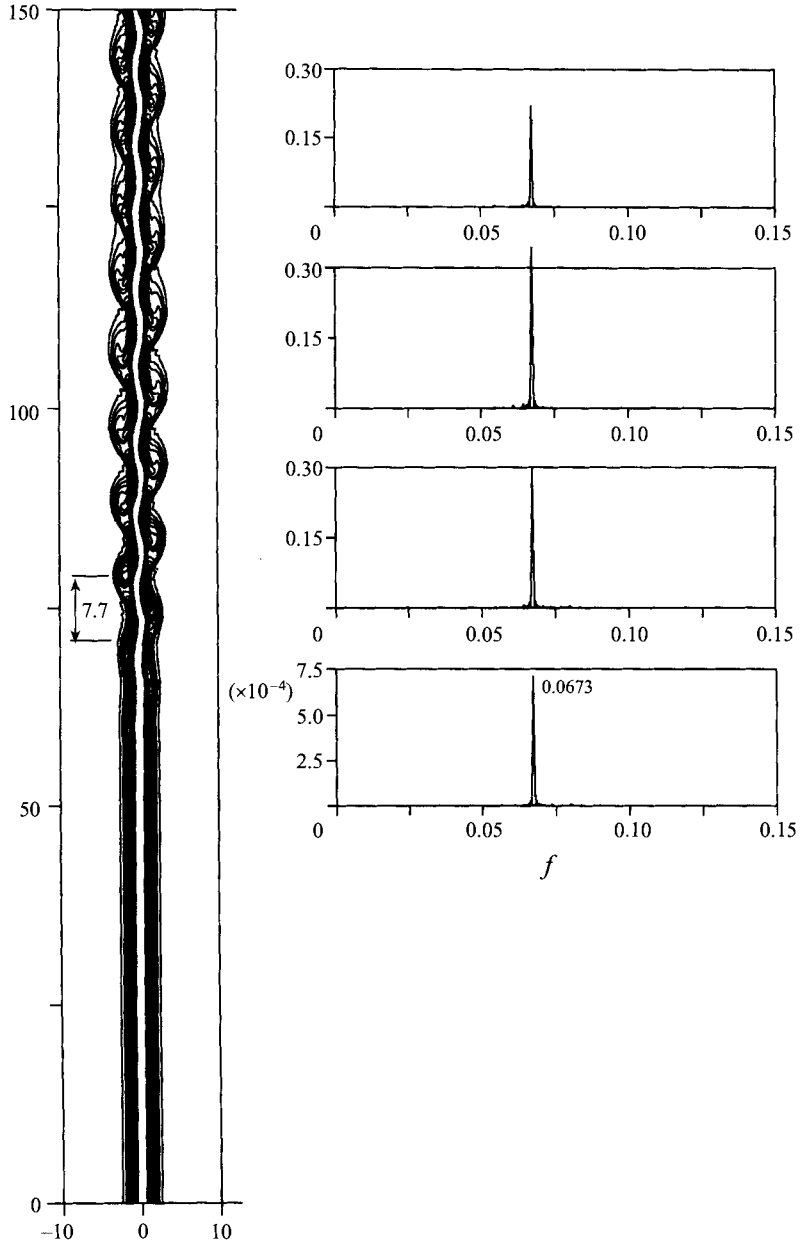

FIGURE 8. Instantaneous isolines of vorticity $\omega(x, y)$ and spectra of $u(x = 0, y)$ at the axial positions $y = 50$, 75, 100, 125 for the reference case $M = 10^3$, $a = 10$ with $Re = 300$.

Figures 8–10 show instantaneous plots of the vorticity field for the reference case with $M = 10^3$, $a = 10$, for three supercritical Reynolds numbers $Re = 300$, 500, 700. Note that for all considered cases the basic stationary, unidirectional solution supposed as inflow boundary condition, is the same. It does not change with Re for a fixed value of M. The figures show isolines of the vorticity ω on the (x, y)-plane. The results have been obtained using a numerical resolution of $n_x = 100$, $n_y = 400$. The discussion focuses on the common features the influence of the Reynolds number.

The flow enters the computational domain with a fully established profile. The two

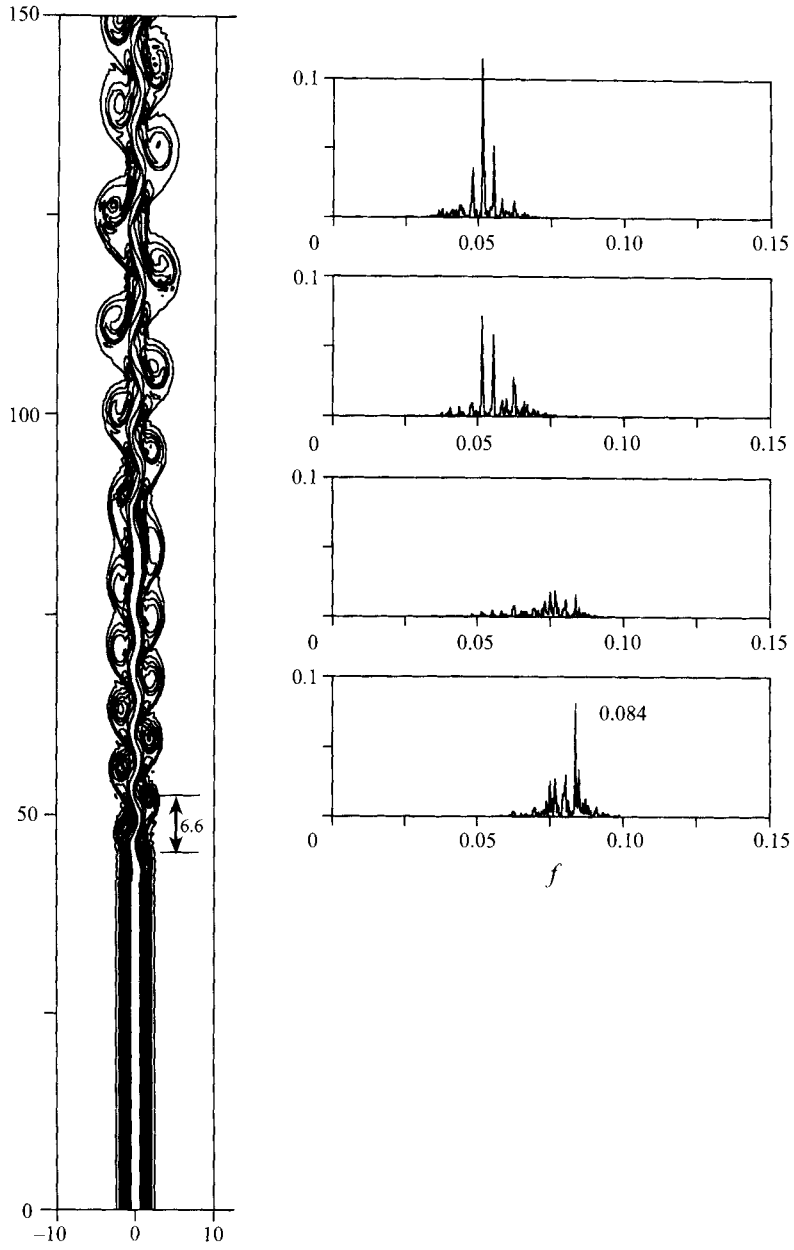

FIGURE 9. Instantaneous isolines of vorticity $\omega(x, y)$ and spectra of $u(x = 0, y)$ at the axial positions $y = 50$, 75, 100, 125 for the reference case $M = 10^3$, $a = 10$ with $Re = 500$.

shear layers at both sides of the conducting strip are parallel and aligned with the main flow direction. They have a maximum and a minimum of ω as already shown in figure 2(*b*). As the fluid moves downstream this basic flow becomes unstable. The first visible instability occurs several characteristic lengthscales downstream. The position y^* where it is observed the first time depends strongly on the Reynolds number; with increasing values of Re, y^* decreases monotonically in the considered range of parameters.

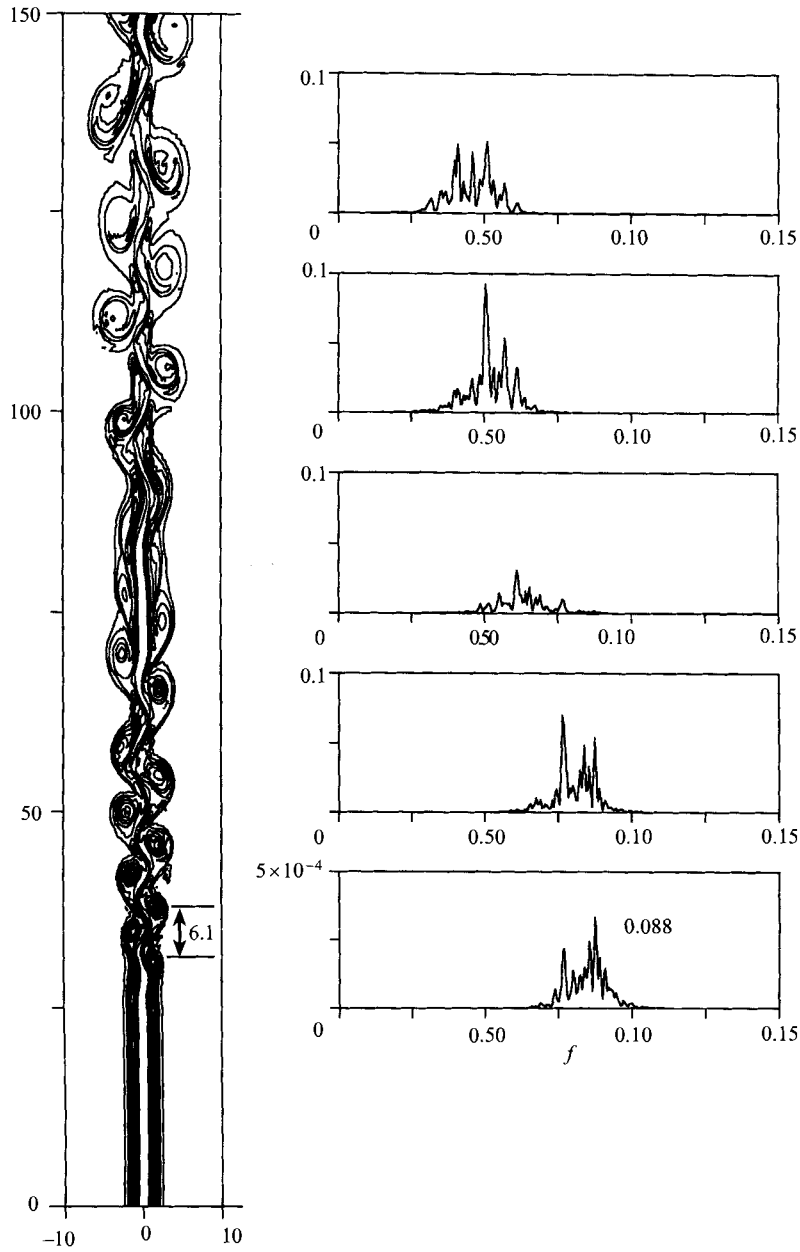

FIGURE 10. Instantaneous isolines of vorticity $\omega(x, y)$ and spectra of $u(x = 0, y)$ at the axial positions $y = 25$, 50, 75, 100, 125 for the reference case $M = 10^3$, $a = 10$ with $Re = 700$.

Some test calculations performed support the idea that the flow is convectively unstable, i.e. an initial perturbation is adverted and grows on its path downstream, while at the position fixed in space, where the perturbation has been initiated the flow remains asymptotically stable. The question arises why nevertheless one can observe instabilities within a finite domain. Using the linear theory for an estimation of the spatial growth rate of the most amplified unstable mode, one can estimate the magnitude of a disturbance near the entrance for which it is necessary that the instability

be amplified to a visible magnitude, say $O(10^{-1})$ at the position y^*. The spatial growth rate k_i is estimated from the temporal one ($\beta = k_r s$) using the transformation proposed by Gaster (1965)

$$k_i = -\frac{\beta_i}{\partial \beta_r / \partial k_r}. \tag{5.7}$$

The value of k_r is varied in order to find the maximum spatial growth rate $k_{i,m}$ at $k_{r,m}$. It turns out that initial disturbances on the order of numerical errors (10^{-7}) are amplified to an order $O(10^{-1})$ after distances of $y^* = 74.3, 42.2, 34.8$ ($k_{i,m} = -0.155, -0.273, -0.330$) for $Re = 300, 500, 700$, respectively. A comparison of these values with y^* taken from figures 8–10 provides a means of explaining the different locations for first visible instabilities at different Reynolds numbers. Moreover, the frequency f_0 and wavelength λ_0 of the first occurring time-dependent structure can be estimated by the linear theory since the first visible instability should correspond to the mode of largest spatial amplification. The frequency $f_0 = \beta_r/2\pi$ and the wavelength $\lambda_0 = 2\pi/k_r$ for $k_r = k_{r,m}$ can be estimated to $f_0 = 0.082, 0.086, 0.088$ and $\lambda_0 = 6.9, 6.4, 6.2$, for $Re = 300, 500, 700$, respectively. The data obtained from the nonlinear numerical analysis suggests values of $f_0 = 0.067, 0.084, 0.088$ and $\lambda_0 = 7.7, 6.6, 6.1$, values which are close to the linear predictions. The comparison between results obtained by linear analysis and by nonlinear numerical calculations show the same tendency and qualitative agreement. The difference between linear predictions and nonlinear analysis is surprisingly small considering the fact that it has been mentioned by Betchov & Criminale (1966) that Gaster's transformation, equation (5.7), may be inaccurate for applications to wake-type profiles.

All these considerations explain the observations (figures 8–10) of the first location of the instability. It is created by very small perturbations due to numerical errors in the fully established profile which has been calculated (as for the linear analysis) and then used as a Dirichlet inflow condition for the nonlinear numerics. The first instability has a frequency and a wavelength close to predictions by the linear analysis for the spatially most amplified mode. Different spatial growth rates for different Reynolds numbers explain the different axial positions where the instability is observed first. The fact that small disturbances near the entrance are the source for the instability does not restrict the results to pure academic considerations, since in any experiment or in engineering applications a perfect inflow will never by realized.

The first appearing instabilities exhibit regular, almost time-periodic vortex patterns comparable to the Kármán vortex street behind bluff bodies. One can consider the Strouhal number

$$St = f\frac{h}{\Delta v}, \tag{5.8}$$

where the non-dimensional frequency f is rescaled with the distance h between the vorticity extrema and the velocity deficit $\Delta v = 1 - v\ (x = 0)$ of the inflow profile. One finds the values $St = 0.15, 0.19, 0.20$, for $Re = 300, 500, 700$, respectively. It is surprising, that these Strouhal numbers are close to those observed for Kármán vortex streets behind circular cylinders in pure hydrodynamic flows, where values between 0.13 and 0.22 are observed, depending on the Reynolds number (see e.g. Lienhard 1966; Cantwell & Coles 1983), although the mechanism of instability is quite different. In the present problem the shear layers become unstable, while Kármán vortex streets are created by a complex interaction of the viscous boundary layers at the cylinder with the near wake.

The main results of the time-dependent reorganization of the flow are summarized in the following sections.

For the smallest Reynolds number considered, $Re = 300$, the characteristic frequency along the axis remains almost constant within the computational domain. It becomes only slightly smaller than the frequency f_0 as shown by the spectra of $u(x = 0, y = 50, 75, 100, 125)$. The vortices are stretched in the axial direction, increasing the wavelength. An exchange of stability or a formation of a secondary street cannot be observed within the finite computational domain for these parameters.

For the Reynolds number $Re = 500$, the situation is more complex. On its path through the computational domain the flow undergoes significant transitions with reorganization to locally regular patterns. The primary vortex street (vortex pattern when the instability reaches visible magnitude) which occurs at $y > y^*$ first increase in transverse extension, while at the same time the intensity of vorticity decreases. The primary street decays further downstream, roughly as $y > 75$. Already at $y = 75$ the characteristic frequency of the primary street $f_0 = 0.084$ no longer plays a dominant role. In the transition region the vortices are stretched in the axial direction. There is a strong interaction between adjacent vortices. Preferential pairing of vortices is observed. The pairing occurs not as in single shear layers, where two vortices of the same size turn around each other to form a larger one. The mechanism here is different. After the axial elongation it seems that stronger vortices survive. There appears to be a suction which transfers vorticity from smaller to adjacent larger vortices. A simple explanation may be that the advection velocity of larger structures is higher than that of smaller ones (one indication supporting this argument is the fact that the phase velocity calculated by the linear theory shows higher values for smaller wavenumbers). However, not all vortices find a suitable partner so that some 'singles' survive.

The transition to new structures agrees widely with observations in the far wake of a circular cylinder where a rapid decay of the initial vortex mode and a formation of a secondary street is also observed. It is reported by several authors that pairing is the leading mechanism for the reorganization (see e.g. Okude & Matsui 1990). Cimbala, Nagib & Roshko 1988 critize the pairing theory; they write that 'with a pairing mechanism the frequency of the secondary street ought to be half that of the primary street'. Since that was not the case in several investigations they conclude that pairing might not be the driving mechanism for the formation of new structures. However, a period doubling would occur only if the advection velocity of the new structure remained unchanged and if the wavelength doubled exactly. This is not the case in our problem and should also not be the case in a developing hydrodynamic wake behind bluff bodies. The occurrence of singles is another explanation for a non-integer frequency ratio between the primary and secondary vortex street, even if the main transition mechanism is pairing.

Although in the present calculations often a pairing of vortices is observed, there are arguments supporting other reorganization mechanisms. Taneda (1959) and, more recently, Cimbala, Nagib & Roshko (1988) and Karasudany & Funakoshi (1994) favour the idea that the secondary vortex street is a result of a new instability of the mean wake after the primary street has decayed to an almost parallel shear flow. The strongest indication for this theory is the fact that in the transition regions neither the frequency of the primary street nor that of the secondary street is found to be dominant. The secondary street therefore exhibits completely new lengthscales and frequencies. The role that the primary street plays is more or less passive. It provides an unstable new mean wake as an initial condition for the secondary street. All these arguments are not in contradiction to our observation of preferential vortex pairing. When the primary

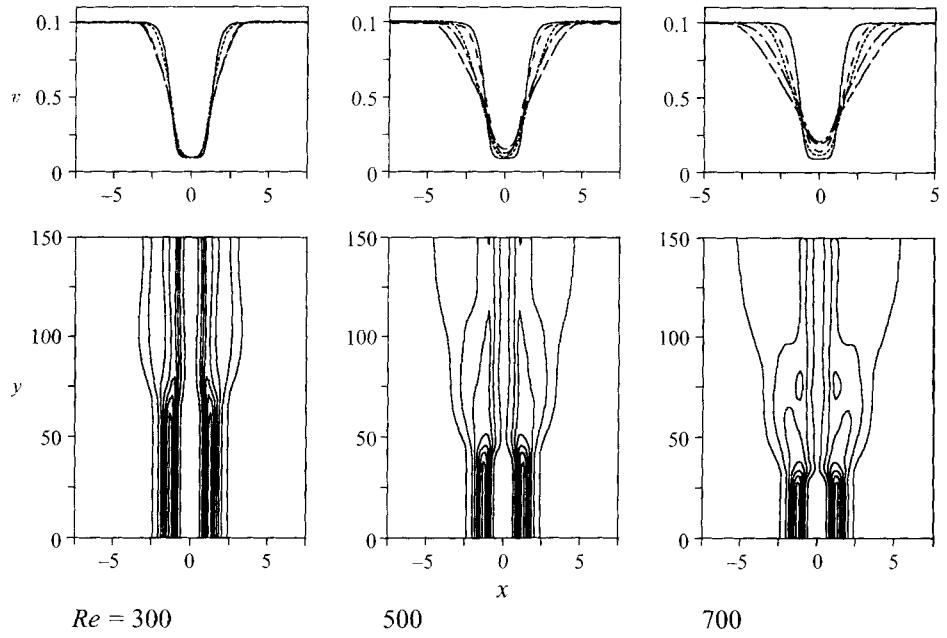

FIGURE 11. Time averaged flow for the reference case $M = 10^3$, $a = 10$, for $Re = 300$, 500, 700. Velocity profiles of the mean wake at the axial positions ——, $y = 25$; – – –, 50; · · ·, 75; – – –, 100; ———, 125 and isolines of mean vorticity.

street decays, the single vortices are elongated and stretched in the axial direction. The shear layers become almost parallel before the pairing takes place. Owing to the axial stretching, the flow finds the possibility of taking new lengthscales, which are more appropriate for the new solution.

From the present results, it does not seem possible to explain the transition to new structures by one or the other theory for the decay of hydrodynamic wakes described in the previous sections. All observed effects can be explained by both hypotheses which do not seem to exclude each other according to the present results.

Another common feature with the hydrodynamic secondary street observed in the far wake of circular cylinders is the fact that it is composed not only by a single prominent frequency. Similar to the experimental observations of Cimbala *et al.* (1988) the secondary street exhibits three outstanding peaks in the spectral amplitude. The occurrence of several frequencies can be explained by observations where an intermittent formation of regular patterns of main scale and frequency are created, which travel as vortex packages along the axis, producing other frequency bands corresponding to the number of vortices per package.

Similar results as described above for $Re = 500$ can be observed for the higher Reynolds number, $Re = 700$. The only difference is that the time-dependent solution is more intense. The spectra show, similar to the previous one, three prominent frequencies except in the transition zone. In this example, the primary street already exhibits three outstanding frequencies. This indicates that even the primary street is composed of several modes before its decay is observed. The decay of the primary street leads to a region of almost parallel shear flow before the secondary street develops.

Besides these time-dependent considerations the time-averaged solution may give an additional insight into the physics of the developing wake. Isolines of the time-

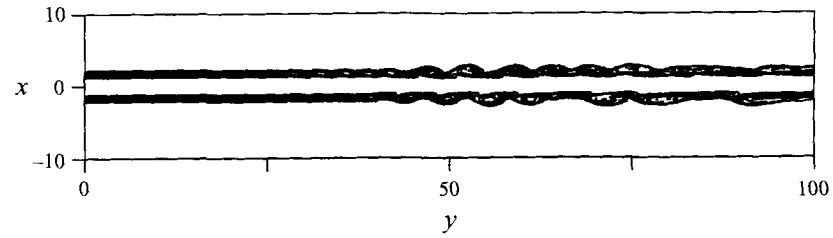

FIGURE 12. Instantaneous isolines of vorticity $\omega(x, y)$ for $M = 10^4$, $a = 10$ with $Re = 5000$.

averaged vorticity are shown in the lower part, and axial velocity profiles of the mean wake at the positions $y = 25, 50, 75, 100$ and 125 in the upper part of the figure 11. The flow at $Re = 300$ exhibits the first instability near $y = 70$. The width of the vortex street increases first. For larger values of y there is a slight contraction of the mean wake before an almost parallel mean flow establishes. For $Re = 500$ the first transition with a lateral expansion occurs for y larger than about 40. The mean wake expands laterally and forms a parallel wake near $y = 70$. It seems as if the solution finds a nonlinear saturation before the secondary transition with larger transverse growth occurs for $y > 80$. Similar behaviour can be seen for $Re = 700$. The first transition here is near $y = 30$, the second near $y = 80$. The total width of the mean wake increases continuously with the Reynolds number.

Many phenomena as described for the reference case $M = 10^3$, $a = 10$, can also be observed for higher values of M once the Reynolds number exceeds the critical value Re_c. For the case $M = 10^4$, $a = 10$, the basic flow becomes unstable for $Re > 1856$ and exhibits more or less time periodic behaviour. One case is shown in figure 12. The frequencies are higher and the wavelengths shorter than for $M = 10^3$. In the reference case there was a strong interaction between the vortices created at both sides of the conducting strip. At the centre $x = 0$ a significant transverse component of velocity u could be observed. For the higher value $M = 10^4$, however, a strong interaction between both vortex strips does not occur. Between the conducting electrodes the vortices are strongly damped so that both unstable shear layers seem to decouple. The vortices cannot extend over larger transverse scales. They are restricted to relatively narrow regions at both initial shear layers. Although time-dependent vortex-type flow patterns are observed the transverse velocity components are only weak. In order to achieve high transverse time-dependent velocities the damping by the electrode should be kept moderate. Such velocities are desirable for fusion applications if the improvement of the transverse exchange of the heat by a vortex-type motion is envisaged. A value of $c_0 = 10/M = 10^{-3}$ seems more effective for the production of larger vortices than the actual one of $c_0 = 10^{-2}$. If $c_0 = 10/M$ is chosen the electrode still conducts much better than the Hartmann layers. This provides the wake-type profile with a sufficiently reduced velocity at the centre, while at the same time the damping remains moderate.

5.3. *Some comments on early and recent experiments*

Experiments reported by Kolesnikov (1972) for the case of two highly conducting electrodes placed in the middle of the Hartmann walls in a channel of rectangular cross-section clearly support the assumptions used in the present theory of a quasi-two-dimensional flow in the core. The experiments show that the assumption $N \gg 1$ made for the present model is not critical. Even for the relatively small interaction parameter of $N \simeq 1.3$ used in his experiment the electric field component in the z-direction had

been constant along z (here the orientation of coordinates are according to the present notation which differs from his original work). From this result he directly concludes that the vorticity in the core does not change along magnetic field lines. Another argument for a quasi-two-dimensional flow is the fact that the intensity ratio of fluctuations of electrical signals measured in the magnetic field direction to those measured in the plane perpendicular to the field is on the order of 10^{-2}, and thus very small. Therefore, there is evidence that the present theory applies even for problems in the range of $N = O(1)$.

In another experiment, Koilesnikov & Tsinober (1972) used non-homogeneous wall conductivities in the form of a pair of conducting circular disks instead of line electrodes. This experiment is indeed quite similar to that described already by Alpher *et al.* (1960), who used an open channel flow with only one conducting disc at the bottom. An attempt to analyses these types of flow with the present model did not show any time-dependent motion if only one pair of conducting disks was used. For high values of N the fluid between the circular electrodes is almost at rest. The electromagnetic forces push the fluid around a column of practically stagnant liquid. Behind the electrodes the fluid was immediately forced to the unidirectional main flow by the strong Lorentz forces. An extended wake behind the electrodes could not be observed, since the inertia forces are weak compared to the Lorentz forces for $N \gg 1$. In the range of lower values of N inertia becomes more important. However, the result is not a developing wake behind the electrodes because the flow does not feel the electrodes at all. The flow passes between the electrodes almost on a straight path. In any considered case no time-dependent motion was observed in the numerical calculations.

The fact that the small fluctuations in the experiment, reported by Kolesnikov & Tsinober (1972) could not be reproduced may be explained by their use of a sharply varying conductivity at the edge of the electrode. There is reason to believe that a sharply changing conductivity of the walls may be responsible for a separate mechanism of instability which is connected to a three-dimensional nature of shear layers (S. Molokov, personal communication). Abruptly changing conductivities of the walls, which would create stronger velocity gradients, are excluded by the assumptions of the present model. Instead of the abrupt change, the conductivity has been varied smoothly, but with strong gradient.

Andreev & Kolesnikov (1993) report an intense transverse convective exchange of fluid in an experiment using a number of conducting spots arranged in the main flow direction. The transverse time-dependent motion improved the heat transfer in this experiment by a factor 5–7 compared to the flow in an insulating duct. This increase cannot be explained by the small fluctuations observed in the early experiments for a single pair of conducting spots. Furthermore, the use of a number of conducting spots, arranged in a line along the main flow direction, should create a wake-type mean profile as in the case of the conducting line electrode, even at lower values of N. If one conducting spot is unable to create a wake a number of them may do so. The mechanism for instability and the time-dependent flow should be comparable to the result discussed earlier in this paper.

6. Conclusions

The modelling of time-dependent MHD flows for fusion relevant parameters, M, $N \gg 1$, becomes important if an improvement of the heat transfer conditions compared with that of laminar inertialess flow is envisaged. Simulations of such flows by three-dimensional numerical codes seem impractical on present day computers since even

calculations for simple stationary problems take hours of computational time, require enormous storage and do not reach the parameters necessary for applications to fusion problems. The asymptotic methods successfully used to describe MHD flows for high M and N have been applied only to inertialess stationary problems up to now. The present paper is an approach to improving on the basic ideas of the asymptotic methods while keeping the weak inertia forces. Owing to the strong electromagnetic forces the inertial flow becomes two-dimensional in the core. Viscous effects are confined to very thin boundary layers at the walls. The basic three-dimensional equations are reduced to set of coupled two-dimensional equations in the plane perpendicular of the magnetic field for the leading variables, the vorticity, the stream function, and the electric potential by an analytical integration along magnetic field lines. The time-dependent two-dimensional equations are solved by efficient numerical methods.

As an example, the flow in a flat channel with passive line electrodes along the main flow direction has been investigated. The electrodes act on the fluid like a brake and thus reduce the velocity locally. The fully developed solution is of the wake type, with a uniform velocity profile some distance from the electrodes and with a reduced velocity between the two electrodes. For Reynolds numbers higher than a critical value Re_c this basic flow becomes unstable. Results for Re_c obtained with the two-dimensional nonlinear model agree well with predictions by a linear stability analysis. For high values of the rescaled Hartmann number $M \gg c^{-1}$, i.e. if the electrodes are much better conducting than the Hartmann layer, Re_c becomes almost proportional to M. With increasing M the wave number k_c and the phase velocity $s_{r,c}$ increase or decrease monotonically and reach values close to 1.5 or 0.5, respectively.

If the flow enters the computational domain with a fully established velocity profile it exhibits the instability after a certain axial distance. The developing nonlinear solution is a result of the spatial amplification of very small deviations from the fully established profile at the entrance. The perturbations grow along the flow path and form finally a vortex street comparable to the Kármán vortex street in the wake of a circular cylinder. With increasing Re the vortex motion is intensified and thus the transverse convective exchange improved. The primary vortex pattern which corresponds to the spatially most amplified mode according to the linear theory decays downstream. A secondary vortex street develops by a recombination, pairing, or merging of primary vortices. The tendency is towards larger scales and towards lower frequencies for larger downstream distances. A recombination to new structures can be observed several times along the axis depending on the physical parameters and on the length of the computational domain. After the primary street has decayed the vortex patterns usually contain contributions of three dominant frequencies.

The result of the present study is that MHD provides an unstable basic velocity profile with two points of inflection. The mechanism for instability seems to be the same as for two-dimensional hydrodynamic flows since most effects found here have already been observed in the hydrodynamic wakes behind bluff bodies. The main difference is the stabilizing effect of the magnetic field. It introduces additional damping in the form of Joules dissipation mainly caused by the high electric currents in the thin Hartmann layers and in the electrodes. This sink reduces continuously the kinetic energy of perturbations and stabilizes the flow.

It has been shown that a vortex-type flow pattern can be established by passive electrical means. The transverse convective exchange should be improved since significant components of velocity in this direction are created by the vortex motion. A further improvement may be achieved if a number of such highly conducting strips

are foreseen in parallel at different x-locations on the walls of the coolant ducts. The vortices can be generated without any mechanical inserts inside the fluid. Besides these simple passive electrodes one can also think of active electrical amplification of vortices by supplying current to the electrodes. According to equation (3.6) such currents should be a source of vorticity. This idea has been already used by Sommeria (1986) in order to create an initial vortex pattern for his studies of the vortex decay, and by Andreev & Kolesnikov 1993 to drive the mean flow in their MHD experiments. It should also be possible to use this idea for the improvement of heat transfer and to apply the present theory for the theoretical predictions.

The author would like to thank Professor U. Müller and Professor J. Sommeria for intense discussions and comments during the preparation of this work.

This work has been performed in the framework of the Nuclear Fusion Project of the Forschungszentrum Karlsruhe and is supported by the European Union within the European Fusion Technology Program.

REFERENCES

ABAS, S. 1969 The effect of a parallel magnetic field on the stability of free boundary-layer type flows of low magnetic Reynolds number. *J. Fluid Mech.* **38**, 243–253.

ALPHER, R. A., HURWITZ, H., JOHNSON, R. H. & WHITE, D. R. 1960 Some studies of free-surface mercury magnetohydrodynamics. *Rev. Mod. Phys.* **32**, 758–769.

ANDREEV, O. V. & KOLESNIKOV, Y. B. 1993 Possibilities of heat transfer intensification to the MHD problems of liquid metal fusion blankets. *Presentation at the Seventh Intl Beer Sheva Seminar on MHD and Turbulence 14–18 Feb 1993* (Proc. to be published in *Magnetohydrodynamics*).

ARAKAWA, A. 1966 Computational design for long-term numerical integration of the equations of fluid motion: Two-dimensional incompressible flow. Part I. *J. Comput. Phys.* **1**, 119–143.

BETCHOV, R. & CRIMINALE, W. O. 1966 Spatial instability of the inviscid jet and wake. *Phys. Fluids* **9**, 359–362.

BÜHLER, L. 1995 Magnetohydrodynamic flows in arbitrary geometries in strong, nonuniform magnetic fields. *Fusion Technology* **27**, 3–24.

CANTWELL, B. & COLES, D. 1983 An experimental study of entrainment and transport in the turbulent near wake of a circular cylinder. *J. Fluid Mech.* **136**, 321–347.

CHANG, C. & LUNDGREN, S. 1961 Duct flow in magnetohydrodynamics. *Z. angew Math. Phys.* **12**, 100–114.

CIMBALA, J. M., NAGIB, H. M. & ROSHKO, A. 1988 Large structure in the far wakes of two-dimensional bluff bodies. *J. Fluid Mech.* **190**, 265–298.

GASTER, M. 1965 The role of spatially growing waves in the theory of hydrodynamic stability. *Prog. Aero. Sci.* **6**, 251–270.

HANNEMANN, K. & OERTEL, H. 1989 Numerical simulation of the absolutely and convectively unstable wake. *J. Fluid Mech.* **199**, 55–88.

HARTMANN, J. 1937 Hg-Dynamics. I. Theory of the laminar flow of an electrically conductive liquid in a homogeneous magnetic field. *DetKgl. Danske Videnskabernes Selskab. Mathematisk-fysiske Meddelelser* **15**(6), 3–28.

HUERRE, P. & MONKEWITZ, P. A. 1985 Absolute and convective instabilities in free shear layers. *J. Fluid Mech.* **159**, 151–168.

HUNT, J. C. R. & MALCOLM, D. G. 1968 Some electrically driven flows in magnetohydrodynamics. Part 2. Theory and experiment. *J. Fluid Mech.* **31**, 775–801.

HUNT, J. C. R. & STEWARTSON, K. 1969 Some electrically driven flows in magnetohydrodynamics. Part 3. The asymptotic theory for flows between circular electrodes. *J. Fluid Mech.* **38**, 225–242.

HUNT, J. C. R. & WILLIAMS, W. E. 1968 Some electrically driven flows in magnetohydrodynamics. Part 1. Theory. *J. Fluid Mech.* **31**, 705–722.

KARASUDANI, T. & FUNAKOSHI, M. 1994 Evolution of a vortex street in the far wake of a cylinder. *Fluid Dyn. Res.* **14**, 331–352.

KOLESNIKOV, Y. B. 1972 Two-dimensional turbulent flow in a channel with inhomogeneous electrical conductivity of the walls. *Magnetohydrodynamics* **8**, 308–312.

KOLESINKOV, Y. B. & TSINOBER, A. B. 1972 Magnetohydrodynamic flow in the region of a jump in the conductivity at the wall. *Magnetohydrodynamics* **8**, 70–74.

LAVRENT'EV, I. V., MOLOKOV, S. YU., SIDORENKOV, S. I. & SHISHKO, A. R. 1990 Stokes flow in a rectangular magnetohydrodynamic channel with nonconducting walls within a nonuniform magnetic field at large Hartmann numbers. *Magnetohydrodynamics* **26**, 328–338.

LEHNERT, B. 1956 An instability of laminar flow of mercury caused by an external magnetic field. *Proc. R. Soc. Lond.* A **233**, 299–310.

LIELAUSIS, O. A. 1975 Liquid-metal magnetohydrodynamics. *Atomic Energy Rev.* **13**, 527–581.

LIENHARD, J. H. 1966 Synopsis of lift, drag and vortex frequency for rigid circular cylinders. *Bulletin 300*, College of Engineering Research Division, Washington State University.

MALANG, S. *et al.* 1988 Self-cooled liquid metal blanket concept. *Fusion Tech.* **14**, 1343.

MOLOKOV, S. & BÜHLER, L. 1994 Liquid metal flow in a U-bend in a strong magnetic field. *J. Fluid Mech.* **267**, 325–352.

MONKEWITZ, P. A. 1988 The absolute and convective nature of instability in two-dimensional wakes at low Reynolds numbers. *Phys. Fluids* **31**, 999–1006.

MOON, T. J., HUA, T. Q., WALKER, J. S. & PICOLOGLOU, B. F. 1992 Liquid metal flow in a simple manifold with a strong transverse magnetic field. *Appl. Sci. Res.* **49**, 49–65.

MOREAU, R. 1990 *Magnetohydrodynamics.* Kluwer.

OKUDE, M. & MATSUI, T. 1990 Vorticity distribution of vortex street in the wake of a circular cylinder. *Trans. Japan Soc. Aeronaut. Space Sci.* **37**, 582–590.

SHERCLIFF, J. A. 1965 *A Textbook of Magnetohydrodynamics.* Pergamon.

SOMMERIA, J. 1986 Experimental study of the two-dimensional inverse energy cascade in a square box. *J. Fluid Mech.* **170**, 139–168.

SOMMERIA, J. & MOREAU, R. 1982 Why, how, and when, MHD turbulence becomes two-dimensional. *J. Fluid Mech.* **118**, 507–518.

TANEDA, S. 1959 Downstream development of wakes behind cylinders. *J. Phys. Soc. Japan* **14**, 843–848.

VERRON, J. & SOMMERIA, J. 1987 Numerical simulation of the two-dimensional turbulence experiment in magnetohydrodynamics. *Phys. Fluids* **30**, 732–739.

WALKER, J. S. 1981 Magnetohydrodynamic flows in rectangular ducts with thin conducting walls. Part I: Constant area and variable area ducts with strong uniform magnetic fields. *J. Méc.* **20**, 79–112.